Caged NADP and NAD. Synthesis and Characterization of Functionally Distinct Caged Compounds †

3 AUTHORS, INCLUDING:

Bruce E Cohen

Lawrence Berkeley National Laboratory

34 PUBLICATIONS **1,501** CITATIONS

SEE PROFILE

Caged NADP and NAD. Synthesis and Characterization of Functionally Distinct Caged Compounds[†]

Bruce E. Cohen,[‡] Barry L. Stoddard,[§] and Daniel E. Koshland, Jr.*[,||]

Departments of Chemistry and Molecular and Cell Biology, University of California and Center for Advanced Materials, Lawrence Berkeley Laboratory, Berkeley, California 94720-3206, and Fred Hutchison Cancer Center, Seattle, Washington 98104

ABSTRACT: Two caged NADP compounds have been synthesized and characterized for use in the crystallographic study of isocitrate dehydrogenase (IDH), as well as for general use in cell biology, metabolism, and enzymology. One caged NADP compound has been designed to be "catalytically caged" so that it can bind to IDH prior to photolysis but is not catalytically active. A second NADP compound is "affinity caged" so that addition of the caging group inhibits binding of the compound to IDH prior to photolysis. The catalytically caged compound was synthesized in a two-step process, starting with the NADase-catalyzed exchange of a synthetic nicotinamide derivative onto NADP. X-ray structures of the NADP compounds with IDH show the catalytically caged NADP bound to the enzyme with its nicotinamide group improperly positioned to allow turnover, while the affinity caged NADP does not bind to the enzyme at concentrations up to 50 mM. Two analogous caged NAD compounds have also been synthesized. The NADP and NAD compounds were characterized in terms of kinetics, quantum yield, and product formation. The affinity caged NADP compound $P^{2'}$-[1-(4,5-dimethoxy-2-nitrophenyl)ethyl] NADP (**VIII**) is photolyzed at a rate of 1.8×10^4 s^{-1} with a quantum yield of 0.19 at pH 7; the NAD analog P-[1-(4,5-dimethoxy-2-nitrophenyl)ethyl] NAD (**IX**) is photolyzed at at a rate of 1.7×10^4 s^{-1} with a quantum yield of 0.17.

Pyridine nucleotides NAD[1] and NADP are the most abundant coenzymes in eukaryotic cells and have long been studied as oxidative cofactors (*1, 2*). The pyridine nucleotides serve as cofactors for all known dehydrogenases and many reductases and hydroxylases, making them the major carriers of H$^+$ and e$^-$ in a number of major metabolic systems, including the glycolysis pathway, the tricarboxylic acid cycle, fatty acid synthesis, and sterol synthesis. The pyridine nucleotides also have an assortment of nonredox functions. NAD serves as the substrate for the mono ADP-ribosylation of host proteins by pathogenic bacteria and for the poly ADP-ribosylation of chromatin. Both NAD and NADP are involved in the phagosomal production of oxygen

radicals in neutrophils and have recently been found to be precursors to compounds involved in a complex process of regulating Ca^{2+} mobilization (*3, 4*).

The importance of the pyridine nucleotides is perhaps best underscored by the extraordinary number of analogs which have been synthesized to study their various functions. To date approximately 200 NADP and NAD analogs have been constructed, including fluorescent derivatives, structural analogs, affinity labels, and spin-labeled analogs (*5, 6*). Missing from this wide-ranging list are caged NAD and NADP. Caged compounds are biologically inactive molecules designed to fragment into biologically active molecules upon photolysis (*7, 8*). As inert compounds, caged molecules can be introduced into biological systems over relatively long periods and then be activated rapidly by light, providing a means of exerting temporal and spatial control over the introduction of physiologically active compounds into complex systems. This approach has proven invaluable in systems where traditional methods of rapid mixing are not possible, such as with membrane preparations, living cells, tissue slices, and protein crystals.

One important application of caged compounds is in determining the structures of short-lived enzymatic intermediates using time-resolved Laue crystallography (*9*). Irradiation of protein crystals soaked with caged compounds can rapidly initiate synchronous turnover within the crystal, allowing catalytic intermediates to be visualized crystallographically. For example, caged GTP has been used to characterize the GTPase activity of Ha-*ras* p21 protein (*10*).

Caged compounds are typically constructed by covalently modifying a biologically active molecule with a photolabile protecting, or "caging", group. Given the function of caged compounds, the key characteristics of an effective caging

* Author to whom correspondence should be addressed.

[‡] Department of Chemistry. Present address: Howard Hughes Medical Institute and the Departments of Physiology and Biochemistry, University of California, San Francisco, CA 94143-0724.

[§] Division of Basic Sciences, Program in Structural Biology, Fred Hutchison Cancer Center, 1124 Columbia Street, Seattle, Washington 98104.

[||] Department of Molecular and Cell Biology and Center for Advanced Materials.

[1] Abbreviations: NADP, nicotinamide adenine dinucleotide phosphate; NAD, nicotinamide adenine dinucleotide; IDH, isocitrate dehydrogenase (*Escherichia coli*); ADP, adenine dinucleotide phosphate; FAB+, fast atom bombardment; NHS, *N*-hydroxysuccinimide; DMF, dimethylformamide; EDC, 1-(3-dimethylaminopropyl)-3-ethylcarbodiimide hydrochloride; CNB, α-carboxy-2-nitrobenzyl; MWCO, molecular weight cut-off; HRMS, high-resolution mass spectrum; DMNPE, 1-(4,5-dimethoxy-2-nitrophenyl)ethyl; DMNB, 1-(4,5-dimethoxy-2-nitrobenzyl); G6PD, glucose-6-phosphate dehydrogenase; ZnTPP, zinc *meso*-tetraphenylporphyrin; MTT, thiazolyl blue; PES, phenazine ethosulfate; DTT, dithiothreitol.

group are its ability to render the substrate inert in the particular system being studied and to then release it rapidly and efficiently following photolysis. In recent years, some extraordinarily fast caging groups have been introduced, including the dimethoxybenzoin (*11*) and 2-methoxy-5-nitrophenyl (*12*) groups, which are capable of microsecond and submicrosecond product release. However, in certain experimental systems the rate-limiting step may be diffusion and binding of the released substrate, not photolysis. These limitations may be particularly acute within a protein crystal, where diffusion rates may be slower and elements of the mother liquor can interfere with the interaction between substrate and target (*13, 14*).

Two biochemically distinct NADP analogs have been constructed for use in the Laue crystallographic study of IDH, an NADP-dependent enzyme of the tricarboxylic acid cycle which converts isocitrate to α-ketoglutarate: one "catalytically caged" NADP compound designed to bind to IDH prior to photolysis but not allow turnover and an "affinity caged" NADP compound designed to have no interaction with IDH prior to photolysis. This paper describes the synthesis and photochemical characterization of these two caged NADP compounds, as well as static X-ray structures of the compounds complexed with IDH both in the dark and following photolysis. The synthesis and characterization of analogous caged NAD compounds are also reported.

EXPERIMENTAL PROCEDURES

Synthesis. Unless otherwise noted, all materials were obtained from commercial suppliers and used without further purification. Organic reaction solvents were dried over 4 Å sieves immediately prior to use. Reverse phase HPLC was performed with a Vydac C_{18} semipreparative column with a Waters model 441 absorbance detector. ^{1}H NMR spectra were determined at 400 or 500 MHz on Bruker superconducting FT spectrometers, and ^{31}P NMR spectra were determined at 162 MHz. The internal reference for ^{1}H spectra was tetramethylsilane; the external reference for ^{31}P NMR spectra was 85% H_3PO_4. Chemical shifts are reported in δ values, positive values indicating shifts downfield from standard. ^{1}H NMR spectra are tabulated in order: multiplicity (s, singlet; d, doublet; t, triplet; m, multiplet; app, apparent), coupling constant(s) in Hertz, and number of protons. FAB+ mass spectra were recorded at the UC Berkeley Mass Spectral Laboratory on an AE1 M512 mass spectrometer. Mass spectral data are reported as *m/z* for the molecular ion. Elemental analyses were performed by the Microanalytical Laboratory, operated by the College of Chemistry, University of California, Berkeley.

*NHS Nicotinate (**II**).* Nicotinic acid (3.00 g, 24.4 mmol) and NHS alcohol (3.10 g, 27.0 mmol) were dissolved in 25 mL of dry DMF. Fresh EDC (5.06 g, 26.3 mmol) was added, and the solution stirred for 10 h under N_2. The solution was concentrated, and the residue partitioned between CH_2Cl_2 and brine. The organic layer was dried, filtered, and concentrated to an off-white solid, which was purified by chromatography on silica gel eluting with ether, affording 5.16 g (96%) of white solid. ^{1}H (CDCl$_3$, 500 MHz): δ 9.30 (d, *J* = 1.7, 1H), 8.87 (dd, *J* = 4.9, 1.7, 1H), 8.37 (app dt, *J* = 8.0,1.8, 1H), 7.46 (ddd, *J* = 7.9, 4.8, 1.7, 1H), 2.90 (s, 4H). Anal. calcd for $C_{10}H_8N_2O_4$: C, 54.55; H, 3.66; N, 12.72. Found: C, 54.24; H, 3.73; N, 12.62.

*(N-Hydroxysuccinimide Nicotinate) Adenine Dinucleotide Phosphate (NHS-NADP, **III**).* NHS nicotinate (1.20 g, 5.46 mmol) was dissolved in 8 mL of acetone and 2 mL of water; this was added to 600 mg (0.78 mmol) of NADP dissolved in 115 mL of 400 mM phosphate buffer, pH 7.2. NADase (1.2 g, 11 units) was added and the mixture shaken at 37 °C. After 30 min, the pH had fallen to 6.9 and was carefully readjusted to 7.1. The reaction was monitored for the loss of NADP by removal of a 10 μL aliquot every half hour for analysis by the glucose-6-phosphate dehydrogenase (G6PD) assay, as described below. After 4 h, the mixture was cooled to 4 °C and spun at 4000*g* for 5 min. The supernatant was concentrated to 40 mL with a rotary evaporator and spun at 12000*g* for 10 min. The supernatant was then added to 180 mL of cold acetone and chilled at −20 °C for 1 h. The precipitate was pelleted at 12000*g*, washed once with cold acetone, and dried under vacuum. This solid was used in the next step without further purification.

*N-(α-Carboxy-2-nitrobenzyl)-nicotinamide Adenine Dinucleotide Phosphate (CNB-NADP, **V**).* A solution of 300 mg (1.19 mmol) of 2-nitrophenylglycine (**IV**) (*15*) in 5 mL of 100 mM phosphate buffer, pH 7.2, was added to half of the crude NHS ester precipitate from the previous reaction (final solution pH = 6.5). The mixture was stirred for 2 h and centrifuged at 4000*g* for 5 min. The supernatant was then passed through an Amicon YM10 ultrafiltration membrane which had been carefully rinsed to remove all NaN$_3$. The filtrate was dialyzed extensively against water (Spectrum dialysis tubing, MWCO 500) and then chromatographed on a DEAE-sepharose column (acetate form), eluting with a linear gradient from 0 to 1 M NH$_4$OAc, pH 5.6. Fractions were assayed for absorbance at 260 nm, showing three main products eluting from the column. Fractions containing the middle product were pooled and lyophilized. The solid was redissolved in H_2O and purified to homogeneity by C_{18} reverse phase HPLC (3 mL/min; 0−10 min, 20 mM NaOAc, pH 5.6; 10−18 min, a linear gradient to 15% MeOH; 18 min onward, 15% MeOH; elution time, 23.3 min). Fractions containing product were concentrated to 20 mL and added to 80 mL of −20 °C acetone, yielding 122 mg (29% from NADP) of precipitate. ^{1}H NMR (D$_2$O, 400 MHz): δ 9.19 (s, 1H), 8.98 (d, *J* = 6.3, 1H), 8.86 (s, 1H), 8.74 (d, *J* = 8.1, 1H), 8.57 (d, *J* = 6.3, 1H), 8.25 (s, 1H), 8.15 (d, *J* = 9.7, 1H), 8.07 (t, *J* = 4.7, 1H), 7.85 (s, 1H), 7.40 (dd, 1H), 6.01 (d, *J* = 6.7, 1H), 5.90 (d, *J* = 4.5, 1H), 5.38 (d, *J* = 5.4, 1H), 4.70 (m, 2H), 4.39 (t, *J* = 5.1, 1H), 4.22−4.04 (m, 5H), 1.73 (s, 3H). ϵ_{355} = 200 M^{-1} cm^{-1}. HRMS (FAB, M·NH$_4^+$): calcd for $C_{29}H_{38}N_9O_{21}P_3$, 941.1395; found, 941.1404.

*N-(α-Carboxy-2-nitrobenzyl)-nicotinamide Adenine Dinucleotide (CNB-NAD, **VI**).* NAD (266 mg, 0.40 mmol) and NHS nicotinate (600 mg, 2.73 mmol) were treated essentially as in the two-step process above. Product was eluted from the DEAE column with a linear gradient from 0 to 600 mM NH$_4$OAc, pH 5.6. Precipitation following purification to homogeneity by C_{18} reverse phase HPLC (3mL/min; 0−10 min, 20 mM NaOAc; 10−17 min, up to 20% MeOH; 17 min onward, 20% MeOH; elution time: 24.4 min) yielded 71 mg of white solid. ^{1}H NMR (D$_2$O, 400 MHz): δ 9.25 (s, 1H), 9.05 (d, *J* = 6.3, 1H), 8.81 (s, 1H), 8.78 (d, *J* = 8.2, 1H), 8.54 (d, *J* = 3.7, 1H), 8.25 (s, 1H), 8.11 (m, 2H), 7.85 (s, 1H), 7.37 (dd, *J* = 8.0,5.1, 1H), 6.07 (d, *J* = 6.6, 1H), 5.85 (d, *J* = 4.2, 1H), 5.40 (d, *J* = 4.2, 1H), 4.49 (d, *J* = 5.2, 1H), 4.32 (d, *J* = 4.2, 1H), 4.26−4.02 (m, 6H), 1.73 (s, 3H). HRMS (FAB, MNa$^+$): calcd for $C_{29}H_{33}N_8O_{18}P_2Na$, 866.1286; found, 866.1271.

$P^{2'}$-[1-(4,5-Dimethoxy-2-nitrophenyl)ethyl] Nicotinamide Adenine Dinucleotide Phosphate (DMNPE-NADP, VIII). NADP (575 mg, 0.75 mmol) was dissolved in 3 mL of H_2O, and the solution was adjusted to pH 4 with 1.0 M NaOH. In a separate flask, 300 mg (1.25 mmol) of 4,5-dimethoxy-2-nitroacetophenylhydrazone (*16*) was stirred in 3 mL of $CHCl_3$ in the dark, and 688 mg (8.00 mmol) of MnO_2 was added. The suspension was stirred for 5 min and then the resulting 1-(4,5-dimethoxy-2-nitrophenyl)diazoethane (**VII**) was filtered through Celite into the stirring NADP solution. The two-phase solution was stirred well in the dark for 2 h. The solution was readjusted to pH 4 with 0.5 M HCl and then **VII** from 100 mg (0.42 mmol) of more hydrazone was filtered through Celite into the solution. The two-phase solution was stirred well in the dark overnight, the organic layer removed, and the aqueous layer washed with $CHCl_3$ (2×3 mL). The aqueous layer was then added to a DEAE anion exchange column (acetate form) and eluted with a linear gradient from 0 to 1 M NH_4OAc, pH 5.8. Fractions were assayed for absorbance at both 266 and 365 nm. Only one series of fractions showed strong absorbances at both wavelengths; they were pooled and concentrated. Analysis by reverse phase HPLC (with elution conditions for **V**) showed a single compound eluting at 28.1 min. To remove excess NH_4OAc, the residue was taken up repeatedly in 95% ethanol and concentrated. The residue was then dissolved in 10 mL of water and added to 200 mL of a 1:1 acetone/EtOH mixture at $-20\,°C$, causing 566 mg (59%) of product to precipitate as a waxy yellow solid. ¹H NMR (D_2O, 400 MHz): δ 9.04 (s, 1H), 8.78 (s, 1H), 8.58 (d, $J = 7.5$, 1H), 8.08 (d, $J = 12.8$, 1H), 7.91 (t, $J = 7.1$, 1H), 7.69 (d, $J = 12.3$, 1H), 7.09 (s, 1H), 6.67 (d, $J = 10.5$, 1H), 5.77 (d, $J = 4.9$, 1H), 5.58 (m, 2H), 4.99 (m, 1H), 4.38 (m, 1H), 4.25 (m, 1H), 4.20 (m, 2H), 4.12 (m, 1H), 4.02–3.95 (m, 4H), 3.64 (m, 6H), 1.19 (d, $J = 6.1$, 3H). ³¹P NMR (D_2O with 50 mM NaOAc, pH 5.8, 162 MHz): δ −1.51, −11.10 (A−B, $J = 20.4$). $\epsilon_{355} = 3900$ M^{-1} cm^{-1}. HRMS (FAB, MH^+): calcd for $C_{31}H_{40}N_8O_{21}P_3$, 953.1521; found, 953.1516.

P-[1-(4,5-Dimethoxy-2-nitrophenyl)ethyl] Nicotinamide Adenine Dinucleotide (DMNPE-NAD, IXa,b). NAD (500 mg, 0.75 mmol) was converted to its tetrabutylammonium salt by passing it over a $(nBu)_4N^+$ AG-1 column, eluting with water. UV-absorbant fractions were pooled and concentrated; the resulting oil was taken up three times in dry DMF and concentrated to a white solid. This solid was stirred in 7.5 mL of dry DMF under N_2. In a separate flask, 359 mg (1.50 mmol) of 4,5-dimethoxy-2-nitroacetophenyl-hydrazone was stirred in 3 mL of $CHCl_3$ in the dark, and 500 mg (5.81 mmol) of MnO_2 was added. The suspension was stirred for 5 min, and then the resulting **VII** was filtered through Celite into the stirring NAD suspension. The $CHCl_3$ was then carefully removed from the mixture with a rotary evaporator. The remaining DMF solution was stirred vigorously in the dark for 18 h, concentrated, and the residue partitioned between 10 mL of $CHCl_3$ and 20 mL of 50 mM NaOAc, pH 5.6. The aqueous layer was washed with $2 \times$ 10 mL of $CHCl_3$ and concentrated to dryness. The yellow residue was resuspended and chromatographed on a DEAE anion exchange column (acetate form), eluting with a linear gradient from 0 to 400 mM NH_4OAc, pH 5.8. Fractions were assayed for absorbance at both 266 and 365 nm. The earlier of two series of fractions showing strong absorbances at both wavelengths was pooled and concentrated. Analysis by reverse phase HPLC (with elution conditions for **VI**)

showed a single broad peak centered at 29.4 min. To remove NH_4OAc, the residue was taken up repeatedly in 95% ethanol and concentrated, and then lyophilized from water, resulting in 370 mg (55%) of yellow oil as a mixture of structural isomers as determined by ³¹P NMR. ¹H NMR (D_2O, 400 MHz): δ 9.10 (s, 1H), 8.92 (d, $J = 5.5$, 1H), 8.59 (d, $J = 7.9$, 1H), 8.12 (s, 1H), 7.97 (d, $J = 6.9$, 1H), 7.75 (s, 1H), 7.10 (d, $J = 11.2$, 1H), 6.92 (d, $J = 10.5$, 1H), 5.86 (d, $J = 5.0$, 1H), 5.71 (d, $J = 5.3$, 1H), 4.47–3.95 (m, 10H), 3.64 (m, 6H), 1.21 (d, $J = 6.0$, 3H). ³¹P NMR (D_2O with 50 mM NaOAc, pH 5.8, 162 MHz): δ −0.44 (m), −10.96 (m). $\epsilon_{355} = 4000$ M^{-1} cm^{-1}. Mass spectrum (FAB+): 907 $(M \cdot NH_4)^+$.

Photolysis. Samples were excited with a Q-switched frequency-tripled Quanta-Ray DCR-11 Nd:YAG laser (55 mJ/8 ns pulse). The actinic light pulse was focused onto the sample cell, a quartz cuvette with a 2 mm excitation path length and a 10 mm detection path length, with a cylindrical lens, forming an ellipse with radii of 2 mm and 7 mm. Samples were prepared to have an absorbance of 0.20 at 355 nm. Transient differential absorption spectra were recorded as the sum of 100 individual laser shots following excitation at 355 nm, with a 100 ns recording delay between excitation and detection. Intermediates were detected using a Hamamtsu xenon arc lamp orthogonal to the actinic beam, which produced two equal-intensity probe beams directed onto the sample by a bifurcated quartz fiber bundle. Each light was detected separately by a Princeton Instruments DIDA-512 Intensified Dual Diode Array Detector, which has a gate duration of 5 ns. Recording delays between laser pulse and probe light were varied with an EG&G 9658 Digital Delay Generator. Ratios of the raw data were found and converted to absorbance.

For quantum yield determinations, laser energies were attenuated by successive addition of borosilicate glass plates between the actinic beam and sample. Energies were measured before each photolysis with a Gentec ED-200 Joulemeter. Samples were prepared with 50 mM phosphate buffer, pH 7.0. The CNB *aci*-nitro anion was monitored at 402 nm; DMNPE intermediates were monitored at 418 nm.

For kinetic experiments, decay of *aci*-nitro intermediates was monitored at 402 or 418 nm with an Osram 50 W tungsten halogen lamp following excitation at 355 nm with a 55 mJ 8 ns pulse. Samples were prepared with 50 mM phosphate buffer, pH 7.0 or 6.0. A total of 256 individual laser shots were averaged for each sample, and the corresponding baseline, recorded without laser excitation, was subtracted for each measurement. Kinetic analysis was made by nonlinear, least-squares computer iteration. The averages of three trials are reported.

Enzymatic Determination of [NADP]. NADP concentrations were determined using G6PD. A 10 μL aliquot of irradiated DMNPE-NADP or of NADase reaction mixture, diluted 100:1, was added to a solution containing 17 μL of MTT (5 mg/mL), 265 μL of PES (1 mg/mL), 250 μL of glucose-6-phosphate (10 mM), 400 μL of 100 mM glycine-glycine buffer (pH 7.4) containing 100 mM nicotinamide, and 33 μL of G6PD (400 units/mL, Sigma).

NADPH formation was monitored as ΔA_{570}/min; a blank rate measured with water instead of the irradiated DMNPE-NADP was subtracted from all measurements. A calibration curve constructed with known concentrations of NADP was used to convert ΔA_{570} rates to [NADP].

Crystallographic Analysis of V and VIII with IDH. IDH was purified (*17, 18*) and crystallized (*19, 20*) as described previously. The crystals were 0.5−1.5 mm along their longest edges, with a shorter third dimension of 0.2−0.3 mm; the crystals belong to space group $P4_32_12$. The unit cell dimensions prior to photolysis and after binding liberated substrate consistently refined to values within 0.5% of the previously published lengths during data processing.

A total of six crystallographic data sets were collected for this study. The structure of the enzyme was determined prior to photolysis after soaking with each compound, in both the presence and the absence of bound isocitrate/Mg^{2+}. The structure of the bound photolysis product was also determined for both caged compounds in the absence of isocitrate/Mg^{2+}.

For each experiment, a crystal was transferred to 0.5 mL of a stabilization solution (generally 10% higher ammonium sulfate than that used to grow the crystals, buffered at pH 7.0 with HEPES) and soaked overnight in the dark with 250 mM of either **V** or **VIII**. These experiments were performed for each compound in the presence and absence of 50 mM isocitrate and MgSO$_4$. To protect the crystal from oxidative degradation after photolysis by the nitroso photoproducts, β-mercaptoethanol (10 mM) and DTT (10 mM) were also added to the mother liquor. The crystals were mounted under safe light in quartz capillaries with mother liquor at either end of the capillary. The mount was sealed with mineral oil and paraffin wax. Initial data were collected at room temperature in the dark on an RAXIS imaging plate area detector with a Rigaku RU-200 rotating anode X-ray generator operating at 50 kV, 80 mA. A complete data set was collected from each crystal to 2.5 Å resolution using 20 1.5° rotations at 30 min per frame, followed by an additional 10 frames collected with the crystal on a 45° jig (Molecular Structure Corporation) for completeness. The total decay in X-ray intensities during collection of each of these four dark data sets was less than 5% of the initial structure average factor amplitudes.

Crystals that were soaked in caged **V** or **VIII** in the absence of isocitrate were each irradiated after the dark data collection, using a two minute exposure with a Cole Parmer 9741-50 quartz halogen light source with a 9741-03 high-intensity 150 W bulb and dual fiber optic light pipes and focusing lenses. The crystal was irradiated from two directions simultaneously, 90° apart in order to maximize efficient excitation of each compound in the crystal lattice. A second data set was then collected after photolysis with an identical strategy to that described above.

For all six final data sets, between 88 and 95% of the unique data were present in the final data set. The internal merging R_{symm} for each crystal and overall R_{merge} between crystals for each individual data set are shown in Tables 1 and 2 and compare favorably with past reported IDH structure determinations (*19−24*). The RAXIS data collection software package (Molecular Structure Corporation) was used to collect and process the data, and all refinements and protein difference Fourier map calculations were conducted with XPLOR (*25*).

The initial coordinates of IDH for refinement and subsequent difference map calculation were the structure of wild-type apoenzyme (*19*) taken from the Brookhaven Protein Data Bank (*26*), with accession number 3ICD. The data were placed into an XPLOR simulated annealing refinement (*25*) using the structure of uncomplexed IDH as the initial

Table 1. Refinement Statistics for IDH−**V** Complexes

	dark (with isocitrate/ Mg^{2+})	dark (without isocitrate/ Mg^{2+})	after photolysis (no isocitrate/ Mg^{2+})
crystal specimen	A	B	B
exposure (h)	15	15	15
rotations (deg)	30 × 1.5	30 × 1.5	30 × 1.5
decay (%)	5	6	7 (13 total)
total reflections	22 695	23 403	23 683
overall R_{symm}^b (%), 2.75−2.5 Å	6.6, 13.2	5.9, 13.1	6.9, 14.5
resolution (Å)	2.5	2.5	2.5
overall $R_{refinement}^c$ (%), 2.75−2.5 Å	19.2, 27.0	19.8, 27.9	20.5, 28.6
overall R_{free}^d (%), 2.75−2.5 Å	22.8, 33.6	23.5, 34.7	24.2, 35.1
structural statistics			
bond distance rms (Å)	0.014	0.015	0.015
bond angle rms (deg)	2.8	2.7	2.6
dihedral rms (deg)	24.3	23.8	23.9

[a] One crystal was used for the data collected in the dark with added isocitrate and Mg^{2+} (specimen A); a second crystal was used for the data collected in the dark and after photolysis in the absence of added isocitrate and magnesium (specimen B). The total exposure time for the first crystal was therefore 15 h (30 frames, 0.5 h each), and for the second crystal was 30 h total (15 h before and 15 after photolysis). The measured decrease in intensities, reported after scaling all frames together, is reported for each data set and as a total percent decay for the second crystal after two consecutive data sets. [b] $R_{symm} =$ initial overall R factor (on intensities) between all symmetry-related reflections in the final merged data set. $R = \sum_j[I_1(j) - I_2(j)]/\sum_j[I(j)]$. [c] $R_{refinement} = \sum_j[F_{obs}(j) - F_{calc}(j)]/\sum_j[F_{obs}(j)]$. [d] $R_{free} =$ agreement between observed and calculated structure factor amplitudes as shown above, calculated for a random distribution of 5% of the reflections that were withheld from all stages of the refinement.

Table 2. Refinement Statistics for IDH−**VIII** Complexes[a]

	dark (with isocitrate/ Mg^{2+})	dark (without isocitrate/ Mg^{2+})	after photolysis (no isocitrate/ Mg^{2+})
crystal specimen	A	B	B
exposure (h)	15	15	15
rotations (deg)	30 × 1.5	30 × 1.5	30 × 1.5
decay (%)	5	6	7 (13 total)
total reflections	23 386	24 006	23 830
overall R_{symm} (%), 2.75−2.5 Å	7.2, 15.9	6.9, 16.1	7.8, 14.2
resolution (Å)	2.5	2.5	2.5
overall $R_{refinement}$ (%), 2.75−2.5 Å	18.2, 29.0	18.8, 28.0	19.4, 29.1
overall R_{free} (%), 2.75−2.5 Å	24.1, 35.9	23.1, 36.1	26.4, 35.9
structural statistics			
bond distance rms (Å)	0.016	0.014	0.016
bond angle rms (deg)	2.4	2.6	2.4
dihedral rms (deg)	22.9	23.8	24.1

[a] Definitions for R factors are the same as in Table 1.

model. Refinement was performed against the data set from 50 to 2.5 Å resolution. A protocol in which the structure, after the initial static energy minimization, is heated to 4000 °C and then immediately placed into a slow cooling (50 ps) annealing minimization was used. No extended dynamics were performed during the heat stage of the refinement.

After this initial round of refinement, difference Fourier syntheses with the coefficients [$F_{o(soaked crystals, dark)} - F_{c(apo enzyme)}$]$\alpha_{calc}$ were calculated using the experimentally measured structure factor amplitudes for the soaked enzyme prior to irradiation. Phases and structure factors for the difference Fourier map were calculated using only the protein model. For those difference maps which showed the
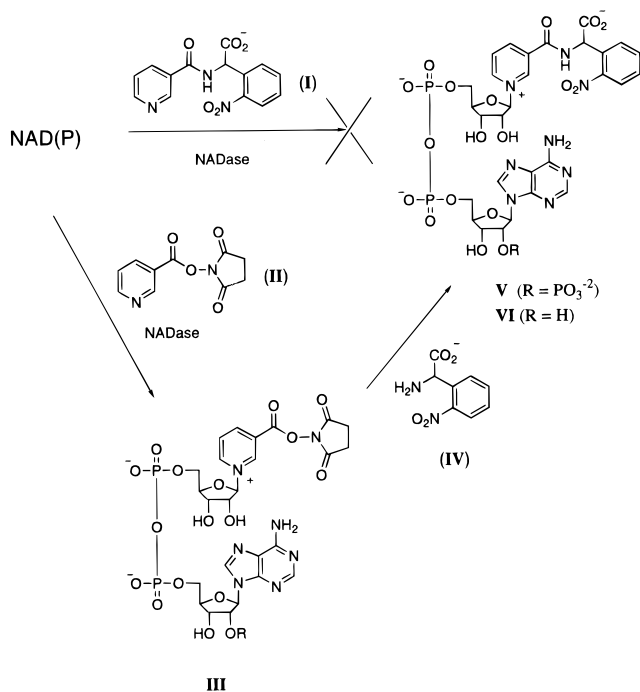
FIGURE 1: Unsuccessful route (as indicated by X, top reaction arrow) and successful route to CNB-NADP (**V**) and CNB-NAD (**VI**) with the NADase exchange reaction through activated ester **III** (R = PO$_3^{-2}$ or H).

presence of bound cofactor before or after photolysis, the visible portions of the molecule were built and the refinement was continued. After a second round of refinement and rebuilding, final residual $F_o - F_c$ difference maps were calculated and examined for any unmodeled density. A small number of water molecules (less than 30 for each structure) were placed, and the refinement was continued. Restrained individual B factors were refined for each structure. Final data and refinement statistics are shown in Tables 1 and 2.

RESULTS

Synthesis of Caged NADP and NAD. The nicotinamide-caged analogs **V** and **VI** were synthesized by an enzymatic reaction using pig brain NADase, a glycohydrolase that is able to catalyze an unusual exchange reaction of synthetic nicotinamide groups onto either NADP or NAD (*27, 28*). Attempts to exchange nicotinamide caged with the α-car-boxy-2-nitrobenzyl group (CNB-nicotinamide, **I**) (Brubaker, M., & Koshland, D. E., Jr., unpublished results) onto NADP with NADase (Figure 1) under a variety of conditions all proved unsuccessful, yielding only starting material and hydrolysis product ADP-ribose phosphate. Nicotinamide-caged CNB-NADP was instead synthesized in a two-step process starting with the NADase-catalyzed exchange of activated ester NHS nicotinate (**II**) onto NADP, yielding NHS-NADP (**III**). Crude **III** was then treated with 2-ni-trophenylglycine, producing caged NADP **V** in 29% yield from NADP. Similar reactions starting with NAD gave **VI** in 21% yield. Proton NMR spectra of both compounds show four additional aromatic resonances corresponding to those expected from 2-nitrophenyl groups, as well as an additional multiplet at δ 5.4 corresponding to the CNB benzylic protons.

The phosphate-caged compounds were prepared by alky-lation of NADP and NAD with diazo compound **VII** (Figure 2), which has shown strong reactivity toward the weakly nucleophilic oxygens of other nucleotide phosphates (*29*).
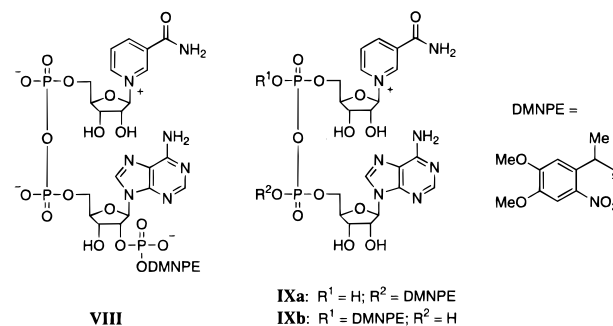

FIGURE 2: Phosphate-caged DMNPE-NADP (**VIII**) and DMNPE-NAD (**IXa,b**).

Diazo compounds have similarly been used to prepare caged derivatives of NAD(P) metabolites cyclic ADP-ribose (*30*) and nicotinic acid ADP (*31*). Oxidation of 4,5-dimethoxy-2-nitroacetophenylhydrazone (*16*) with MnO$_2$ in CHCl$_3$ produced the highly labile and photosensitive **VII**, which was filtered directly into a stirring solution of NADP, producing DMNPE-NADP (**VIII**, Figure 2). The ^{1}H NMR spectrum of the major product of this reaction purified by anion-exchange chromatography shows two additional aro-matic resonances compared to the NADP spectrum and three new methyl groups corresponding to the aromatic methoxy groups and benzylic CH$_3$. A ^{31}P NMR spectrum shows an upfield shift of 1.7 ppm for the 2′-phosphate resonance compared to NADP, while the diphosphate resonances remain unchanged. These data, along with ^{1}H NMR peak integration and mass spectral data, are indicative of the addition of a single caging group at the 2′-phosphate.

Because the backbone diphosphate oxygens are unreactive toward **VII** under the biphasic reaction conditions used to prepare **VIII**, NAD was alkylated in aprotic organic solvent, conditions which have been reported to increase the reactivity of more strongly acidic phosphate groups (pK_a < 4) toward diazo compounds (*32, 33*). As determined by ^{1}H NMR peak integration, the purified product again shows the addition of a single caging group; a new resonance at δ −0.44 in the ^{31}P NMR spectrum corresponds to an alkylated backbone phosphate group. The broadness of this peak and the δ −10.96 peak of the unalkylated phosphate suggest a mixture of expected structural isomers **IXa** and **b**.

Photochemical Characterization

Transient Absorption Spectra. Figure 3a shows the differential absorption spectra of nicotinamide-caged CNB-NADP and phosphate-caged DMNPE-NADP following excitation by 355 nm laser pulse. The broad absorption peaks in the 400−420 nm range are characteristic of the *aci*-nitro anions (**X**, Figure 4) produced following photolysis of 2-nitrobenzyl compounds. Transients from the DMNPE compound shows peak absorbances at 418 nm, while the CNB transient is centered at 402 nm.

Quantum Yield. For nicotinamide-caged CNB-NADP, the quantum yield for formation of the *aci*-nitro anion (Φ$_a$) was calculated by measuring the transient absorbance as a function of laser energy, as has been described (*34*). Previous studies have shown that product formation follow-ing photolysis of 2-nitrobenzyl compounds correlates well with *aci*-nitro anion formation and decay (*29, 35, 36*). Laser energies were attenuated by the introduction of increasing numbers of glass plates between the laser and the sample cell, and absorbances measured at 402 nm. A well-
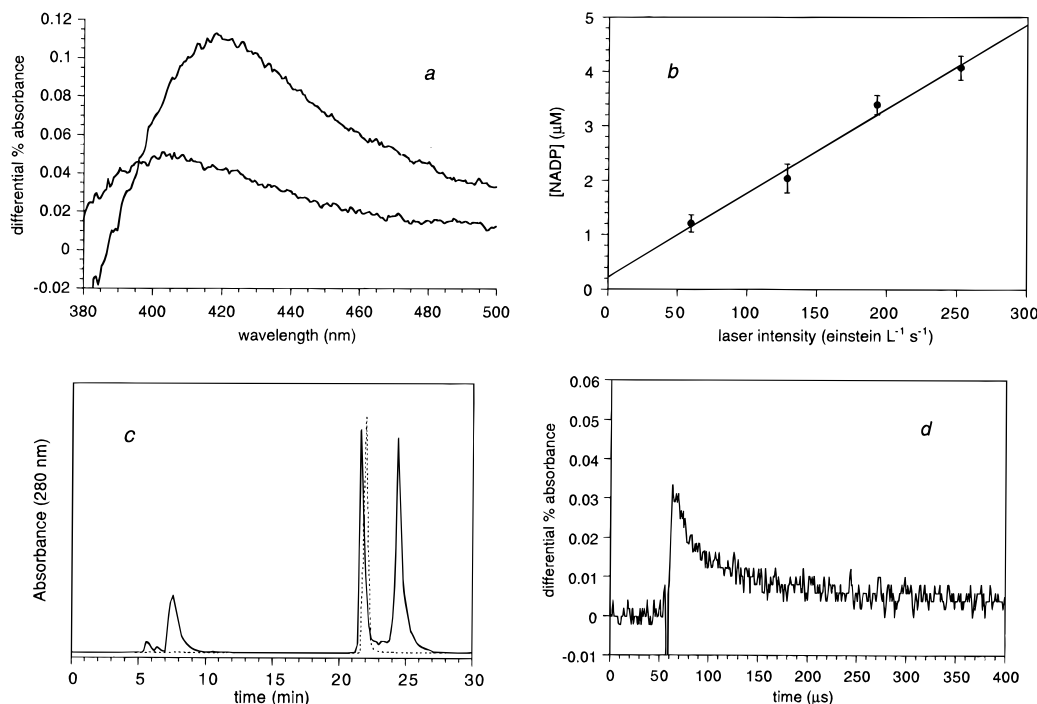
FIGURE 3: Photochemical characterization of caged pyridine nucleotides: (a) Transient absorption spectra of **V** and **VIII** following a 355 nm laser pulse. The spectrum of **VIII** has a maximum of 418 nm, while the spectrum of **V** has a maximum of 402 nm. (b) NADP concentration as a function of laser intensity. Samples of **VIII** were irradiated and the resulting NADP concentrations determined with glucose-6-phosphate dehydrogenase. (c) C$_{18}$ HPLC traces of a partially photolyzed sample of **VI** (solid line) and commercially available NAD (dotted line). (d) Absorbance at 418 nm following photolysis of **VIII**, pH 7, with 100 mM DTT.
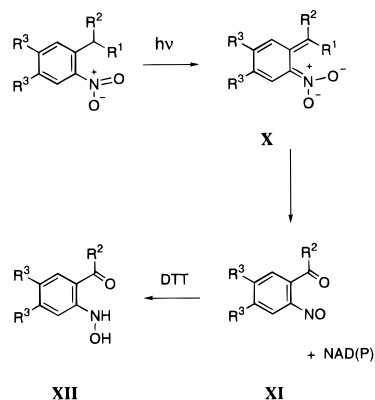
FIGURE 4: General mechanism of photocleavage of 2-nitrobenzyl-caged compounds, via *aci*-nitro anion **X** to nitrosoketone **XI**. In the presence of DTT, **XI** is reduced to **XII**. R^1 is NADP or NAD. For compounds **V** and **VI**, R^2 = CO$_2^-$ and R^3 = H. For compounds **VIII** and **IX**, R^2 = Me and R^3 = OMe.

characterized standard, formation of the ZnTPP triplet at 470 nm, was used to calibrate laser energies. Using these data, as well as literature values of 2600 M^{-1} cm^{-1} for ϵ_a of CNB (37) and 74000 M^{-1} cm^{-1} and 0.83 for ϵ_{ZnTPP} and Φ_{ZnTPP} of ZnTPP (34), Φ_a is calculated to be 0.09.

Quantum yields for DMNPE-caged compounds **VIII** and **IX** cannot similarly be calculated because no value for the extinction coefficient of the DMNPE *aci*-nitro anion has been reported. The product quantum yield of **VIII** was instead calculated by measuring the NADP concentrations of samples irradiated at varying laser intensities (Figure 3b). Samples were irradiated as described for **V**, and NADP concentrations of these samples were determined with the G6PD assay, which is capable of measuring picomolar concentrations of NADP (38, 39). Using this method, the quantum yield of NADP formation following photolysis of **VIII** was determined to be 0.19.

This value of Φ_p was in turn used to calculate ϵ_a for the DMNPE *aci*-nitro intermediate and Φ_a for DMNPE-caged NAD (**IX**). Transient absorbances of both DMNPE-caged compounds were determined as functions of laser energy, yielding a value of ϵ_{418} for the DMNPE *aci*-nitro anion of 8600 M^{-1} cm^{-1}. Using this value, Φ_a for **IX** was calculated to be 0.17.

Identification of Photolysis Products. Three methods were used to confirm that the caged compounds described in this paper produce NAD(P) following photolysis. For the CNB-caged compounds (**V** and **VI**), formation of NADP and NAD was confirmed by reverse phase HPLC analysis of solutions of irradiated caged compounds (Figure 3c). The HPLC trace of a partially photolyzed sample of **V** contains a new peak with a retention time of 11.1 min, which corresponds to the retention time of commercially available NADP. The CNB-NAD trace similarly includes a new peak at 21.9 min corresponding to NAD. Both traces include new peaks at 7.5 min, the reported retention time of the ketoacid photoproduct (**XI**) under similar elution conditions (37). As noted above, photolyzed phosphate-caged DMNPE-NADP was active with G6PD, providing evidence that NADP is formed from that caged compound. Finally, NADP is present in X-ray structures (described below) of IDH with either photolyzed **V** or **VIII**.

Kinetics. The rates of photorelease for compounds **V**, **VIII**, and **IX** were determined by measurement of the rates of decay of the *aci*-nitro anions produced following photolysis. The spectral changes at 418 nm following photolysis of **VIII** are shown in Figure 3d. Photolyzed DMNPE-caged samples all showed a rapid rise in absorbance characteristic of *aci*-nitro anion formation, followed by decays which were best fit to double-exponential functions. Photolysis of **VIII** in the presence of 10 mM DTT produced a transient with decay rates of 1.3×10^4 and 93 s^{-1}. Raising [DTT] to 100

mM increased the slow component 5-fold to 480 s^{-1} while only marginally increasing the fast component to 1.8×10^4 s^{-1}. DMNPE-NAD showed a fast decay component of 1.7×10^4 s^{-1}.

The transient produced by photolysis of **V** exhibited first-order decay kinetics at rates considerably slower than those for **VIII** ($k = 30$ s^{-1}). Decrease of the sample pH to 6 marginally increased the rate of photorelease to 42 s^{-1}, which is consistent with literature reports of a mild pH dependence of k for CNB-caged compounds (*37*).

X-ray Crystallography

IDH-V Stuctures. Electron density maps of the enzyme active site prior to photolysis, with Fourier coefficients $[F_{o(\text{soaked crystals,dark})} - F_{o(\text{apoenzyme})}]\alpha_{\text{calc}}$ clearly indicate the presence of bound **V** both with and without bound isocitrate/Mg^{2+}. In both cases, the nicotinamide ring is disordered as previously described (*23*). In the absence of bound isocitrate (Figure 5A), the only observable atoms of **V** are the adenine ring, its adjoining 2′-phosphoribose, and the first backbone phosphate. This last phosphate is only weakly ordered, as shown by the quality of the density in that region and by its behavior in the refinement. In the presence of bound isocitrate (Figure 5B), observable density is present for the entire bound caged NADP up to the ribose immediately preceding the nicotinamide ring. The results of the final refinements of data sets for IDH with **V** are shown in Table 1.

IDH-VIII Stuctures. Electron density maps of the enzyme active site prior to photolysis clearly reveal the absence of bound **VIII**, even at contour levels approaching the noise level of the map. In the presence of isocitrate/Mg^{2+}, the substrate and metal are bound as an active site complex as previously described (*19*), while the caged compound is still not visible (Figure 5D). In the absence of bound isocitrate, the only observable features in the difference map of the active site are a pair of peaks that are probably a pair of loosely associated phosphate ions from the crystal mother liquor (Figure 5E). The results of the final refinements of all three data sets of IDH with **VIII** are shown in Table 2.

IDH Structures with Photolysis Products of V or VIII. Difference maps of the enzyme after photolysis of either **V** or **VIII** (Figures 5C and 5F), with Fourier coefficients $[F_{o(\text{after photolysis})} - F_{o(\text{before photolysis})}]\alpha_{\text{calc}}$, are identical to maps previously reported for bound complexes of either NADP or NADPH (*23, 24*) confirming that the compound binds through interactions with the adenine ring after photolysis, with a disordered phosphate backbone, ribose, and nicotinamide ring. They are also identical to maps calculated for the IDH-**V** complex prior to photolysis, confirming that the enzyme binds to **V** in the dark through interactions with the adenine ring and neighboring phosphoribose. These structures confirm earlier data showing that NADP is produced following photolysis of either **V** or **VIII**.

DISCUSSION

Design and Synthesis. Designing molecules as either catalytically or affinity caged compounds, in particular, designing an NADP derivative which can bind to IDH without allowing turnover, required detailed information about IDH-NADP interactions. Data from both the IDH-NADP X-ray structure (*23*) and from competition experiments with NADP analogs (Mesecar, A., & Koshland, D.

E., Jr., unpublished results) indicate that the nicotinamide is not tightly bound by the enzyme. On the basis of these data, modification of the nicotinamide should result in smallest disruption to IDH binding of any NADP functionality; at the same time, it is most likely to disrupt catalysis because the nicotinamide ring serves the reactive center of the cofactor. For construction of a catalytically caged NADP, the nicotinamide group is then an ideal location for placement of the caging group. For construction of an affinity-caged NADP, these studies indicate that incorporation of a caging group at the 2′-phosphate should most significantly reduce the affinity of NADP for IDH.

The inability of NADase to utilize the CNB-caged nicotinamide (**I**) as a substrate may be due to steric factors, as **I** is larger than the largest reported NADase substrate, 3-benzoylpyridine, which has been shown to undergo NADase-catalyzed exchange only in very low yields (*40*). This limitation was circumvented by use of activated ester **II**, which provided a handle for introducing the CNB group. The NHS-NADP intermediate (**III**) has the potential to be elaborated into a variety of other compounds, effectively overcoming the steric limitation of the NADase-exchange reaction and greatly expanding its scope. For example, **III** could potentially be attached to amino linkers on beads for use in affinity chromatography.

Photochemical Properties. Transients from DMNPE compounds **VIII** and **IX** show peak absorbances at 418 nm, while the CNB transient following photolysis of **V** is centered at 402 nm. Although a thorough literature search reveals no transient absorption spectrum previously published for the DMNPE *aci*-nitro anion, the related DMNB intermediate has been found to have an absorbance maximum of 420 nm (*41*). For the CNB *aci*-nitro transient, the peak absorbance of 402 nm is blue shifted significantly from the wavelength of 435 nm originally reported by Milburn et al. (*37*) in their characterization of CNB. It is instead consistent with the unidentified slower component centered at 406 nm which has been reported for several *N*-linked CNB compounds (*7, 12, 42, 43*). The photolysis rates of **V** also correspond well with this unidentified intermediate, which has been reported to have a decay rate of 25 s^{-1}. No evidence of the faster 435 nm transient also seen in these studies was observed in the present experiments. The shifting of the transient peak absorbance may be due to the strongly electron-withdrawing nature of the positively charged nicotinamide ring. This would be expected to at least partially offset the electron-donating effects of the carboxylate group, which itself shifts the peak wavelength from 406 nm (for the unsubstituted 2-nitrobenzyl *aci*-nitro anion) to 435 nm for CNB. The 402 nm centered peak may also be associated with a transient other than the *aci*-nitro anion, as has been hypothesized (*7*).

Formation of these *aci*-nitro transients was used to determine quantum yields of the caged compounds, while their decay rates were used to determine the rates of photorelease. For DMNPE-caged compounds, the use of *aci*-nitro decay to measure product release rates is complicated by the DMNPE nitrosoketone photoproduct (**XI**), which absorbs strongly at 418 nm (*44*). Radical scavengers such as thiols have been shown to react with the nitrosoketone to form **XII**, eliminating its absorbance in that wavelength range (*45*). The slow component of the decay of **VIII** varies with [DTT] while the fast component does not, indicating that this fast component represents the decay of the *aci*-nitro
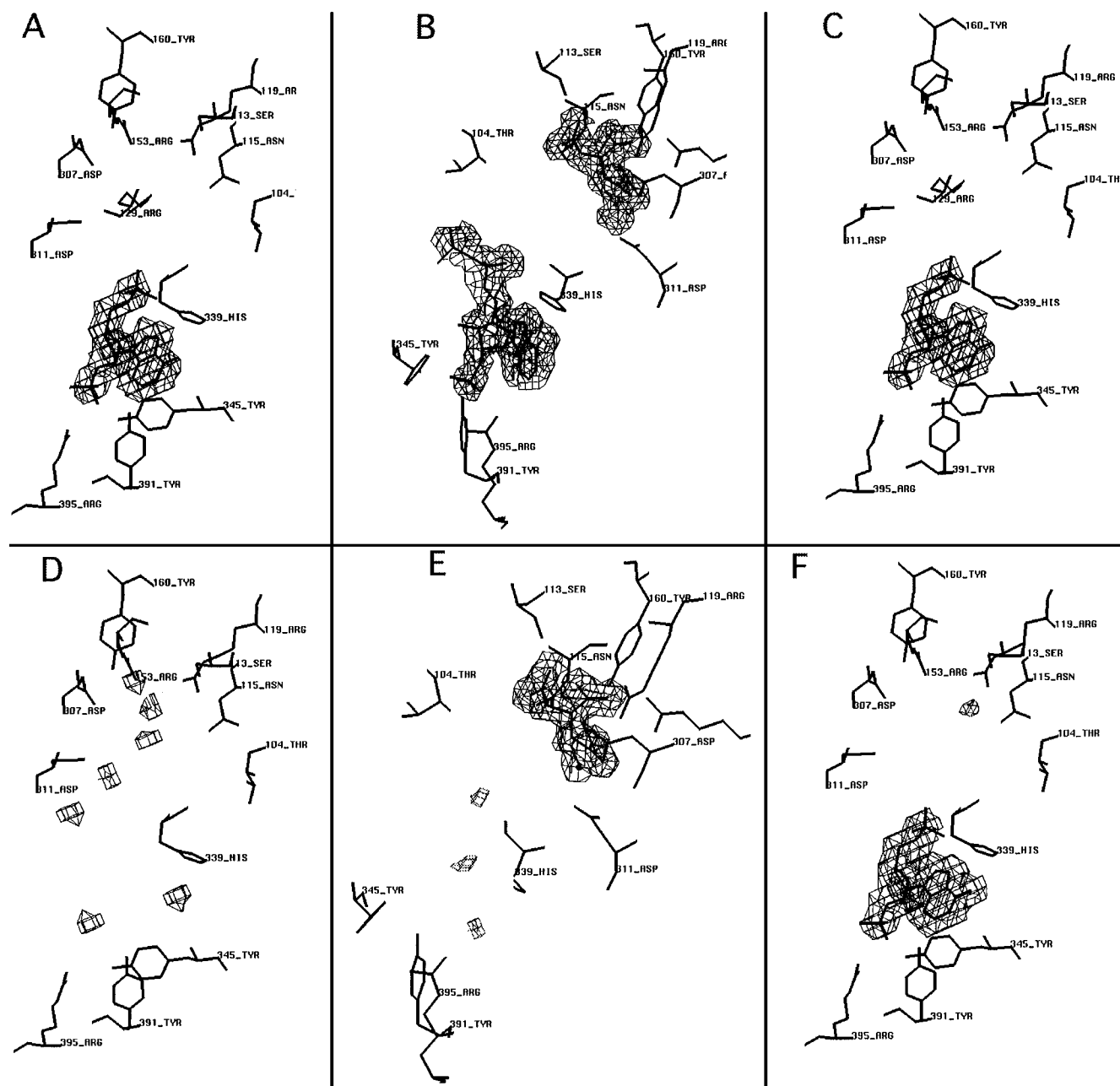
FIGURE 5: Crystallographic studies of CNB-NADP (**V**) and DMNPE-NADP (**VIII**) with IDH. Nicotinamide-caged compound **V** binds to the enzyme through interactions between the adenosyl ring and adjoining phosphoryl-ribose, as previously shown for unmodified NADP (*23*) (panel A). The nicotinamide ring, its ribose sugar, and the first backbone phosphate are all completely disordered. When the same caged compound (**V**) is soaked into crystals in the presence of bound isocitrate/Mg^{2+}, both backbone phosphates of the caged cofactor are well ordered in a difference map (panel B), indicating that the nicotinamide group and its ribose are more strongly attracted to its binding site in the presence of the substrate. The presence of the caging group on the carboxyamide nitrogen sterically prevents hydride transfer. The fact that turnover does not occur under these conditions (through the presence of contaminating bound NADP) was verified by absorbance analysis of dissolved crystals after extensive soaks (B. L. Stoddard, unpublished data), as well as by the fact that the crystals do not crack or dissolve (which is indicative of turnover for this system). After photolysis in the absence of isocitrate, liberated NADP is still bound to the active site as previously determined for unmodified NADP (panel C). The clear advantage of this compound as a photolytic trigger for time-resolved studies is that it is bound to the enzyme active site prior to photolysis, so that no additional diffusion or binding events are necessary to form the Michaelis complex. Additional studies conducted in the crystal with compound **V**, flash-photolyzed in the presence of isocitrate/Mg^{2+}, demonstrate that the liberation of the caging group on the nicotinamide carboxyamide leads to production of product (B. L. Stoddard, unpublished studies). Phosphate-caged compound **VIII** fails to bind to IDH when soaked into crystals in the absence (panel D) or presence (panel E) of bound isocitrate/Mg^{2+}. Photolysis of the compound in the crystal, however, generates a normal enzyme–NADP complex (panel F). This compound, although both fast and extremely efficient for photodissociation, must bind to the enzyme active site after release as part of the mechanism of catalytic triggering. All figures are of $F_o - F_c$ difference Fourier omit maps calculated at the end of refinement. All panels contoured at 2σ density, except for panels D and E, which are contoured at 1σ to more closely examine the map for bound cofactor. Features of electron density are excluded from the regions of the enzyme side chains for clarity, but are otherwise unmodified.

anion to the nitrosoketone photoproduct, while the slow component represents the rate of reaction of the photoproduct with DTT. The rate of this DTT-nitrosoketone reaction is similar to the rates of other thiol-nitroso reactions which have been reported. McCray and Trentham (*44*) determined the second-order rate constant for the reaction of dithioerythritol with the 2-nitrobenzyl photoproduct to be 3.5×10^3 M^{-1} s^{-1}. At a thiol concentration of 100 mM, this corresponds to a decay rate of 350 s^{-1}, a value similar to the slow component observed in the present experiments.

The rates of NADP and NAD formation from DMNPE-caged compounds **VIII** and **IX** are similar to the rate of photolysis of DMNPE-caged phosphate (*33*), but considerably faster than the rates of DMNPE-caged ATP (*33*) and glycine (*16*) photolysis. They are also significantly faster than the turnover rate of IDH within the crystal at pH 7 [38 s^{-1}; (*13*)], indicating that the rate of photolysis for **VIII** will not be a limiting factor in triggering synchronized IDH turnover. Use of the DMNPE caging group seems to have been largely abandoned following the initial reports of disappointing photochemical characteristics for DMNPE-ATP and DMNPE-glycine. However, the experiments reported here indicate that DMNPE-caged compounds are capable of rapid release rates and extensive product formation, and that their use warrants further investigation.

For general use, the phosphate-caged DMNPE compounds offer definite advantages over the nicotinamide-caged CNB compounds. In addition to having a much faster photolysis rate, DMNPE-NADP's quantum yield and is about twice that of CNB-NADP, and its value of ϵ_{355} is 20-fold greater. Taken together, these two pieces of data indicate that an approximately 400-fold lower concentration of **VIII** than **V** would be required to produce the same concentration of NADP following excitation at 355 nm.

As seen in Figure 3b, a final concentration of 4.1 μM NADP is produced at the full laser energy of 55 mJ following a total of 800 ns of excitation of **VIII**. This represents photorelease of 72% of the caged NADP in the elliptical cylinder irradiated by the actinic beam.[2] Similar values for Φ and ϵ_{355} were observed for DMNPE-caged NAD (**IX**), indicating that significant amounts of NADP and NAD can be released from the DMNPE-caged compounds on very short time scales.

One other notable feature of the plot in Figure 3b is that it does not pass through the origin, indicating that some NADP is present in the sample even in the absence of any photolysis. The least-squares fit of the data intersects the *y* axis at an NADP concentration of 0.2 μM, or 0.4% of the sample. This impurity is presumably caused by hydrolysis of the phosphate ester; other DMNPE-caged nucleotides have also been reported to be prone to hydrolysis (*33*). Even at these low levels, the presence of free NADP could potentially interfere with certain applications of the caged compound, suggesting that **VIII** should be used as quickly as possible following purification. For systems requiring absolutely NADP-free caged compound, application of NADase immediately prior to use is also a potential method for removing any stray NADP. A similar method of using alkaline phosphatase was recently reported to remove uncaged substrate from a nicotinic acid ADP preparation (*31*). For the present study, it is worth noting that the chemical instability of **VIII** is not sufficient to interfere with the 8 h crystallographic experiment described below.

Biochemical Characterization. Structures of catalytically caged compound **V** with IDH in the absence of isocitrate/Mg^{2+} show that the caged cofactor is bound in a manner identical to underivatized NADP (*23*). However, the pseudo-Michaelis complex of IDH-**V**-isocitrate/Mg^{2+} differs from the previously described pseudo-Michaelis complex of IDH-NADP-isocitrate/Ca^{2+} (*20*), and the Laue Michaelis structure of the Y160F IDH mutant with NADP and isocitrate/Mg^{2+} (*13*) in that the nicotinamide ring is spatially disordered. It also differs significantly from attempts to form the Michaelis complex of IDH-NADP-isocitrate/Mg^{2+}, as exposure to both isocitrate/Mg^{2+} and NADP causes IDH crystals to crack or dissolve (*20*). The simplest interpretation of these data is that in the absence of bound isocitrate, the nicotinamide ring and its neighboring atoms are repelled strongly by a number of charged side chains in the active site, whereas when isocitrate/Mg^{2+} are bound, these side chain charges are effectively neutralized, allowing the nicotinamide moiety to bind to the enzyme. However, when the CNB caging group is attached to the nicotinamide group, as in **V**, the nicotinamide ring is prevented from properly approaching its binding site. The nicotinamide ring therefore appears disordered, and the absence of an active cofactor prevents turnover and cracking in the crystal.

The presence in Figure 5B of the substrate isocitrate, and not product α-ketoglutarate, also indicates that the enzyme is not capable of turnover with **V** as its cofactor. The caged compound is thus bound but not active, providing confirmation of the catalytic caging strategy. These structures show that placement of caging group on the nicotinamide group displaces it sufficiently to impair its catalytic activity, while allowing the rest of the molecule to retain its affinity for IDH. For affinity-caged NADP, the absence of the caged cofactor from crystals soaked with **VIII** indicates that placement of the caging group on the 2′-phosphate effectively destroys any interactions between the compound and the enzyme.

These results suggest that, despite its rapid rate of photorelease, in an IDH crystal the rate of reaction initiation by photolyzed **VIII** may limited by diffusion and binding of NADP to the active site. While this may be sufficiently fast to produce homogeneous accumulation of enzymatic intermediates,[3] the only reported Laue experiment utilizing a caged substrate in which short-lived enzymatic intermediates could be resolved has been the study of p21 GTPase activity, in which caged GTP was found to bind to the protein prior to photolysis (*10*). In contrast, a similar Laue experiment with glycogen phosphorylase *b* and caged phosphate failed to resolve catalytic intermediates (*46*); it has been proposed that the rate of reaction in this case was limited by diffusion of liberated phosphate, because photolysis of the caged compound was confined to the outer regions of the crystal, where most of the uncaging radiation was absorbed (*14*). The X-ray structures in Figure 5 demonstrate that compound **V** has been successfully designed to behave in a manner similar to caged GTP in the p21 study, binding to IDH prior to photolysis and eliminating any potential delay caused by diffusion and binding of NADP.

The strategy of adding photolabile groups to biomolecules has been an invaluable resource since Hoffmann and co-workers introduced caged ATP in 1978 (*47*). The work reported here demostrates that the strategic addition of caging groups can also be used confer biochemical properties specifically tailored to affect the utility of the caged compound.

REFERENCES

1. Dolphin, D., Poulson, R., and Avramovic, O. (1987) *Pyridine nucleotide coenzymes: chemical, biochemical, and medical aspects*, Wiley, New York.
2. You, K.-S., Anderson, B., and Everse, J. (1982) *The Pyridine Nucleotide Coenzymes*, Academic Press, New York.
3. Lee, H. C., Graeff, R., and Walseth, T. F. (1995) *Biochimie 77*, 345−355.
4. Aarhus, R., Dickey, D. M., Graeff, R. M., Gee, K. R., Walseth, T. F., and Lee, H. C. (1996) *J. Biol. Chem. 271*, 8513−8516.
5. Anderson, B. M. (1982) in *The Pyridine Nucleotide Coenzymes* (Everse, J., Anderson, B., and You, K.-S., Eds.) pp 91−133, Academic Press, Inc., New York.
6. Woenckhaus, C., Jeck, R. (1987) in *Pyridine nucleotide coenzymes: chemical, biochemical, and medical aspects* (Dolphin, D., Poulson, R., and Avramovic, O., Eds.) pp 449−567, Wiley, New York.
7. Corrie, J. E. T., Trentham, D. R. (1993) in *Bioorganic Photochemistry Volume 2: Biological Applications of Photochemical Switches* (Morrison, H., Ed.) pp 243−305, John Wiley & Sons, Inc., New York.
8. Adams, S. R., Tsien, R. Y. (1993) *Annu. Rev. Physiol. 55*, 755−784.
9. Moffat, K., Szebenyi, D., and Bilderback, D. (1984) *Science 223*, 1423−1425.
10. Schlichting, I., Almo, S. C., Rapp, G., Wilson, K., Petratos, K., Lentfer, A., Wittinghofer, A., Kabsch, W., Pai, E. F., Petsko, G. A., and Goody, R. S. (1990) *Nature 345*, 309−315.
11. Trentham, D. R., Corrie, J. E. T., and Reid, G. P. (1992) *Biophys. J. 61*, A295.
12. Niu, L., Wieboldt, R., Ramesh, D., Carpenter, B. K., and Hess, G. P. (1996) *Biochemistry 35*, 8136−8142.
13. Bolduc, J. M., Dyer, D. H., Scott, W. G., Singer, P., Sweet, R. M., Koshland, D. E., Jr., and Stoddard, B. L. (1995) *Science 268*, 1312−1318.
14. Mozzarelli, A., and Rossi, G. L. (1996) *Annu. Rev. Biophys. Biomol. Struct. 25*, 343−365.
15. Davis, A. L., Smith, D. R., and McCord, T. J. (1973) *J. Med. Chem. 16*, 1043−1045.
16. Wilcox, M., Viola, R. W., Johnson, K. W., Billington, A. P., Carpenter, B. K., McCray, J. A., Guzikowski, A. P., and Hess, G. P. (1990) *J. Org. Chem. 55*, 1585−1589.
17. Reeves, H. C., Daumy, G. O., Lin, C. C., and Houston, M. (1972) *Biochim. Biophys. Acta 258*, 27−39.
18. LaPorte, D. C., Thorsness, P. E., and Koshland, D. E., Jr. (1985) *J. Biol. Chem. 260*, 10563−10568.
19. Hurley, J. H., Thorsness, P. E., Ramalingam, V., Helmers, N. H., Koshland, D. E., Jr., and Stroud, R. M. (1989) *Proc. Natl. Acad. Sci. U.S.A. 86*, 8635−8639.
20. Stoddard, B. L., Dean, A., and Koshland, D. E., Jr. (1993) *Biochemistry 32*, 9310−9316.
21. Hurley, J. H., Dean, A. M., Sohl, J. L., Koshland, D. E., Jr., and Stroud, R. M. (1990) *Science 249*, 1012−1016.
22. Hurley, J. H., Dean, A. M., Thorsness, P. E., Koshland, D. E., Jr., and Stroud, R. M. (1990) *J. Biol. Chem. 265*, 3599−3602.
23. Hurley, J. H., Dean, A. M., Koshland, D. E., Jr., and Stroud, R. M. (1991) *Biochemistry 30*, 8671−8678.
24. Stoddard, B. L., and Koshland, D. E., Jr. (1993) *Biochemistry 32*, 9317−9322.
25. Brunger, A. T., Kuriyan, J., and Karplus, M. (1987) *Science 235*, 458−460.
26. Bernstein, F. C., Koetzle, T. F., Williams, G. J., Meyer, E. E., Jr., Brice, M. D., Rodgers, J. R., Kennard, O., Shimanouchi, T., and Tasumi, M. (1977) *J. Mol. Biol. 112*, 535−542.
27. Zatman, L. J., Kaplan, N. O., and Colowick, S. P. (1953) *J. Biol. Chem. 200*, 197−212.
28. Colowick, S. P., and Kaplan, N. O. (1957) *Methods Enzymol. 4*, 840−855.
29. Walker, J. W., Reid, G. P., McCray, J. A., and Trentham, D. R. (1988) *J. Am. Chem. Soc. 110*, 7170−7177.
30. Aarhus, R., Gee, K., and Lee, H. C. (1995) *J. Biol. Chem. 270*, 7745−7749.
31. Lee, H. C., Aarhus, R., Gee, K. R., and Kestner, T. (1997) *J. Biol. Chem. 272*, 4172−4178.
32. Nerbonne, J. M., Richard, S., Nargeot, J., and Lester, H. A. (1984) *Nature 310*, 74−76.
33. Wootton, J. F., and Trentham, D. R. (1989) in *NATO Advanced Research Workshop on Photochemical Probes in Biochemistry* (Nielsen, P. E., Ed.) pp 277−296, Kluwer Academic Publishers, Boston.
34. Hurley, J. K., Sinai, N., and Linschitz, H. (1983) *Photochem. Photobiol. 38*, 9−14.
35. McCray, J. A., Herbette, L., Kihara, T., and Trentham, D. R. (1980) *Proc. Natl. Acad. Sci. U.S.A. 77*, 7237−7241.
36. Walker, J. W., McCray, J. A., and Hess, G. P. (1986) *Biochemistry 25*, 1799−1805.
37. Milburn, T., Matsubara, N., Billington, A. P., Udgaonkar, J. B., Walker, J. W., Carpenter, B. K., Webb, W. W., Marque, J., Denk, W., McCray, J. A., and Hess, G. P. (1989) *Biochemistry 28*, 49−55.
38. Bernofsky, C., and Swan, M. (1973) *Anal. Biochem. 53*, 452−458.
39. Nisselbaum, J. S., and Green, S. (1969) *Anal. Biochem. 27*, 212−217.
40. Dietrich, L. S., Friedland, I. M., and O., K. N. (1958) *J. Biol. Chem. 233*, 964−974.
41. Walker, J. W., Martin, H., Schmitt, F. R., and Barsotti, R. J. (1993) *Biochemistry 32*, 1338−1345.
42. Wieboldt, R., Gee, K. R., Niu, L., Ramesh, D., Carpenter, B. K., and Hess, G. P. (1994) *Proc. Nat. Acad. Sci. U.S.A. 91*, 8752−8756.
43. Ramesh, D., Wieboldt, R., Billington, A. P., Carpenter, B. K., and Hess, G. P. (1993) *J. Org. Chem. 58*, 4599−4605.
44. McCray, J. A., and Trentham, D. R. (1989) *Annu. Rev. Biophys. Biophys. Chem. 18*, 239−270.
45. Goldman, Y. E., Gutfreund, H., Hibberd, M. G., McCray, J. A., and Trentham, D. R. (1982) *Biophys. J. 37*, 125a.
46. Duke, E. M. H., Hadfield, A., Walters, S., Wakatsuki, S., Bryan, R. K., and Johnson, L. N. (1992) *Trans. R. Soc. London, Ser. A 340*, 245−261.
47. Kaplan, J. H., Forbush, B. D., and Hoffman, J. F. (1978) *Biochemistry 17*, 1929−1935.